

Less is More: The Influence of Pruning on the Explainability of CNNs

David Weber¹, Florian Merkle^{2,3}, and Pascal Schöttle³ Stefan Schlögl³

MCI – The Entrepreneurial University, Universitätsstr. 15, 6020 Innsbruck, Austria
 {d.weber,f.merkle,p.schoettle,s.schloegl}@mci.edu.de

Abstract. Modern, state-of-the-art Convolutional Neural Networks (CNNs) in computer vision have millions of parameters. Thus, explaining the complex decisions of such networks to humans is challenging. A technical approach to reduce CNN complexity is network pruning, where less important parameters are deleted. The work presented in this paper investigates whether this technical complexity reduction also helps with perceived explainability. To do so, we conducted a pre-study and two human-grounded experiments, assessing the effects of different pruning ratios on CNN explainability. Overall, we evaluated four different compression rates (i.e., CPR 2, 4, 8, and 32) with 37 500 tasks on Mechanical Turk. Results indicate that lower compression rates have a positive influence on explainability, while higher compression rates show negative effects. Furthermore, we were able to identify sweet spots that increase both the perceived explainability and the model’s performance.

Keywords: Explainable AI · Neural Network Pruning · Artificial Intelligence

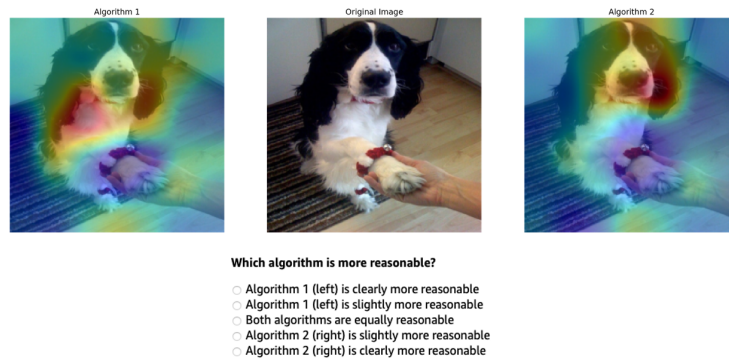


Fig. 1: Which algorithm is more reasonable? In the middle, we show the original picture; on the left, the explainability heat-map of compression rate 1; and on the right, the explainability heat-map for compression rate 8. Red colors indicate more important regions while blue colors indicate less important regions.

1 Introduction

Today’s products and services increasingly benefit from the integration of ever more powerful machine learning (ML) features. In particular, the use of ‘deep learning’, and respective deep neural networks (DNN), has significantly expanded upon the capabilities of intelligent systems and consequently improved the performance of autonomous vehicles, virtual assistants, fraud detection software, as well as tools that make heavy use of image recognition technology. Concrete application domains for these DNNs are found, e.g., in medicine [34], production [53], cyber security [4] and finance [32]. To this end, convolutional neural networks (CNN) – a particular type of DNN – have demonstrated great performance in computer vision tasks. This includes image classification of chest x-rays to treat COVID-19 patients [17], image segmentation of MRI scans to analyze different regions of the brain [5], or object detection to support autonomous driving [52]. Yet, although DNNs (and consequently CNNs) show great performance in the above-outlined tasks, they face two major limitations:

1. **Complexity:** State-of-the-art DNNs have to deal with millions of parameters and thus require large amounts of computing power and memory. This is especially important for applications in resource-constraint environments, such as smartphones and IoT devices. Furthermore, a higher number of parameters negatively influences the inference time, which is critical for real-time applications such as autonomous cars or face detection. One technical approach to retrospectively reduce DNN parameters is so-called neural network pruning, where less important parameters are deleted.
2. **Explainability:** DNNs experience a lack in explainability that leaves little understanding on why a particular decision was made [21]. Especially the structure of CNNs, consisting of complex internal relations, can be difficult to explain [8]. Understanding the reasoning of these systems is crucial, especially for high-stake decision-making and highly regulated domains. Here, the DNN’s decisions may determine the difference between life and death, as in healthcare, medicine, or autonomous driving. More explainable, reasonable, and transparent DNNs would therefore increase trust, acceptance, and awareness in society.

Intuitively, more parameters, i.e., more complexity, lead to a lower explainability, simply because not every connection can be interpreted with human reasonability. This is clearly shown with DNN’s, as their high number of parameters and complex internal sequences appear opaque to humans [12] and certain explainability methods are prone to produce noisy and indistinct explanations [35].

At the same time, this strive for complexity definitely helped state-of-the-art NNs reach their current performance. In this paper, we start from the hypothesis that retrospectively reducing the number of parameters with the help of NN pruning can increase the explainability to humans.

We applied several network pruning compression rates (CPR), i.e. CPR 2, 4, 8, and 32, to a VGG-16 [65] network. VGG-16 is a widely applied CNN

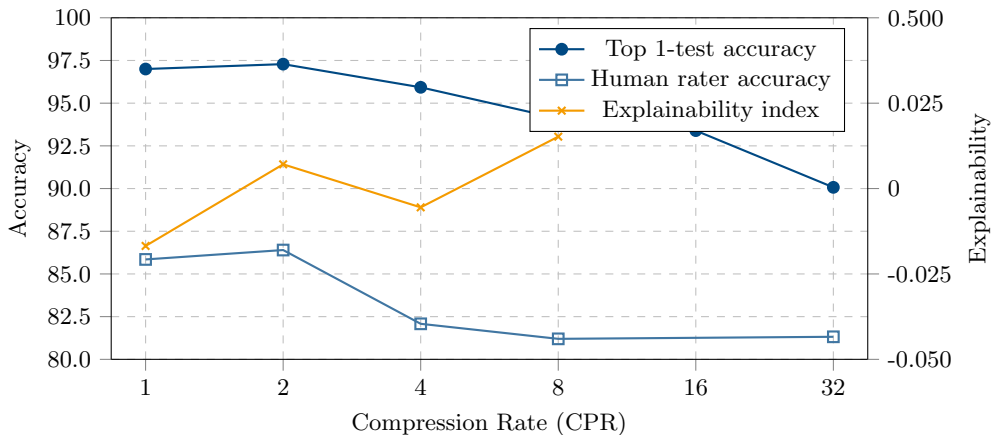


Fig. 2: Top-1 test-set accuracies (dark blue, left y-axis), human rater accuracies (light blue, left y-axis), and our explainability measure (orange, right y-axis) for different CPRs.

architecture that consists of a simple and homogeneous structure. Its size of 138 million parameters provides ideal preconditions for pruning and opaque behavior. Grad-CAM [63] was our explainability method of choice, as it provides a visual explanation for the internal reasoning of black-box CNNs, passes several sanity checks by [3], and is applicable to any CNN architecture.

In total, we executed three human-grounded experiments with 37 500 tasks on Amazon’s Mechanical Turk platform. We analyzed the data gathered from these experiments with subjective and objective evaluation metrics. Figure 1 shows the experimental setup of one of our experiments. Our results indicate a sweet spot of mild pruning, with a CPR of 2, i.e., a CNN with half the number of parameters. As visible in Figure 2, not only the top 1 test accuracy of the CNN improved, but also both, the subjective (explainability index) and objective evaluation metric (human-rater-accuracy). The remainder of this paper reports the details of this investigation.

We start with a discussion of the relevant theoretical background in Section 2. Next, we describe our methodological approach in Section 3. Section 4 then reports on respective results, Section 5 reflects on the limitations of our approach, and Section 6 highlights directions for future work. Finally, Section 7 summarizes and concludes the paper.

2 Theoretical Background

ML methods, in particular DNN approaches, are powerful tools for creating predictions based on data. Yet, they are often called black-box models, as their

inner-workings lack transparency. Even so, these non-transparent systems are increasingly used for high-stake decision-making in healthcare, precision medicine, criminal justice, autonomous driving and other highly regulated domains impacting human lives [57, 7, 70]. Not being able to explain the system’s decisions thus poses evident dangers [2]. This implies that it is not enough to receive a prediction (i.e., the *what*), but also the explanation of how this prediction was made (i.e., the *why*). Or, as [18] emphasize, “*Explainability completes the problem formulation*”.

2.1 Explainability in Machine Learning

Unfortunately, ML literature lacks a clear definition of *explainability* and *interpretability*. Consequently, terms are regularly ill-defined, misused or referred to in different ways [39]. Also, it may happen that *explainability* and *interpretability* are used synonymously [13, 46], although [24] clearly state that *interpretability* (i.e., human-understandability) and *fidelity* (i.e., the accurate description of a system’s internal workings) are required to reach *explainability*. Several definitions for *interpretability* exist. Some refer to it as the ability to explain technology in human-understandable terms [18, 49], which in turn brings forth the question of what understandable means. [54], on the other hand, define interpretability as the extent to which “*a user is able to obtain true insights into how actionable outcomes are obtained*” and split the concept into the subproperties *clarity* and *parsimony* [54, p. 6]. High *clarity* is achieved when the explanation is unambiguous, while high *parsimony* is achieved when the explanation is perceived as simple by the user, which depends on their capabilities. Fidelity generally describes whether an explanation is accurate. [37] divide fidelity further into *soundness* and *completeness*, where *soundness* describes whether the explanation is correct and faithful to the task model, and *completeness* is achieved when the explanation covers the entire dynamic of the task model.

ML explainability supports the social acceptance of, trust in, and social interaction with ML systems, and fosters their safety and knowledge acquisition [56]. That is, the systems’ safety may be increased through increasing its explainability [46], and so is the possibility for identifying faulty behavior, as more explainable systems may ease testing, auditing and debugging [48]. Furthermore, explainability helps people to successfully interact with ML systems and eventually reach intended goals [48]. In short, ML explainability supports researchers and practitioners alike and at the same time helps extract the ‘knowledge’ a system uses [48]. Finally, the European Union’s *Right to Explanation* [25] demonstrates the regulatory importance of humanly explainable ML systems, aiming to achieve equality and unbiased decision-making by algorithms [24]. [16] support these efforts by defining the concept of *Socially Responsible AI Algorithms* and providing four fundamental responsibilities: functional, legal, ethical, and philanthropic.

2.2 Methods of CNN Explainability

[26] describes the *black-box explanation problem* as the challenge to provide an explanation of the black-box model through an interpretable system or method. The difficulty lies in providing insights about the internal processes that lead to a DNN’s prediction and further clarifying under which circumstances they can be trusted [54] and producing insights into model predictions [55]. DNNs may have millions of parameters, making it hard to analyze their internal representations and the respective information flow throughout the network. Their complex learning procedure is determined by many components, including regularization, activation, and loss functions. Specifically, CNNs entail complex internal relations due to their structure. They consist of sequences of convolutional and pooling layers that learn increasingly higher-level features. The challenge here is to reduce the complexity of these operations, which is usually done by visualizing saliency maps [24]. In theory, it should be easier for humans to understand CNNs than regular DNNs that do not make use of convolutional layers, as our cognitive skills favour the understanding of this type of visual data [8]. This assumption has led to the definition of model-agnostic [42, 56] as well as model-specific methods, both of which aim to help with explanations for CNN decisions. Model-agnostic methods are applied to any ML algorithm and are usually applied after the model has been trained - post-hoc [14]. While these methods analyze pairs of feature input and output, they do not have access to the inner information of the analyzed models [49]. Common methods in use are Local Interpretable Model-Agnostic Explanations (LIME) [56] and Shapley Values (SHAP) [42]. Model-specific methods either map the output back to the given input or explain the representation of the external world inside the layers [8, 24]. Most of the model-specific methods fall into the first category. Perturbation-based methods deliver good estimates of the input pixels’ impact, yet induce high computational costs [6]. Hence, backpropagation-based methods are commonly used, e.g. [67, 64, 77, 62], as they compute the attributions with one or few forward and backward passes resulting in less computational costs [6].

Class Activation Mapping (CAM) Proposed by [76], Class Activation Mapping (CAM) is a weakly supervised method for classification-trained CNNs to perform object localization. As such, CNNs do not have to be trained with bounding box annotations. CAM rather highlights the discriminating object parts in an image; and since important image regions are highlighted, it also helps explain the CNN’s decision. It applies global average pooling on the final convolutional feature maps and is only applicable to architectures consisting of several convolutional layers and one single fully connected layer producing predictions, e.g., GoogLeNet [68].

Generally, CAM projects the weights of the output layer back to the feature maps, allowing for the identification of important image regions [76]. The last convolutional layer (= penultimate CNN layer) produces K feature maps $A^k \in \mathbb{R}^{u \times v}$ of width u and height v . The localization maps $L_{\text{CAM}}^c \in \mathbb{R}^{u \times v}$ for each

class c are then created by linearly combining the learned weights of the final layer w_k^c and the final feature maps A_k .

$$L_{\text{CAM}}^c = \sum_k w_k^c A^k$$

The produced activation map has the size of the last convolutional layer’s feature maps A^k . In order to use them for model visualization and explainability, these maps are then up-scaled to the size of the input image and normalized between zero and one.

Gradient-weighted Class Activation Mapping Grad-CAM, proposed by [63], is one of the most prominent backpropagation-based attribution methods. Grad-CAM applies post-hoc to any CNN-based architecture and enables class-discriminative visualization. As shown by [43] and [10], very deep convolutional layers capture instance-specific information and different types of image structures. Spatial information is then lost in the following fully-connected layers. Therefore, deep convolutional layers represent the best option to capture higher-level semantics and spatial information. Grad-CAM aims to capture these high-level semantics and detailed spatial information from the network in order to identify image parts that were important for the classification decision. Similar to CAM, Grad-CAM uses the feature maps of the last convolutional layer. To calculate the Grad-Cam heat-map, first the gradient of the score for the respective image class y^c is calculated with respect to the activation map (outputs) A of the chosen target convolutional layer (commonly the last convolutional layer), i.e. $\frac{\partial y^c}{\partial A_{ij}^k}$. Global average pooling then yields a vector α_k^c with a weight for each channel of the activation map.

$$\alpha_k^c = \overbrace{\frac{1}{Z} \sum_i \sum_j}^{\text{global average pooling}} \frac{\partial y^c}{\partial A_{ij}^k}$$

Next, the activation map A^k is multiplied with the weight vector α_k^c and all channels are summed up, producing a heat-map with the same height and width as the convolutional layer output. Finally, a *ReLU* operation is performed, canceling out all below-zero values. Similar to CAM, also Grad-CAM up-samples and normalizes the resulting heat-maps for visualization.

$$L_{\text{CAM}}^c = \text{ReLU} \left(\sum_k \alpha_k^c A^k \right)$$

2.3 Evaluating Explainability

Evaluating ML explainability has a two-fold goal [44]: First, it assesses if explainability is achieved. Here, the focus of the evaluation lies in determining whether

the provided explainability method achieves the defined objective [39]. Second, it aims to formally compare available explainability methods and consequently identify preferences. One of the biggest challenges therefore lies in the evaluation itself, as no ground truth is given [60, 55]. This is especially true for post-hoc explainability methods, where one attempts to explain the inner workings of a black-box model. Finally, the ultimate target is to assess to what extent all properties of explainability are satisfied [44].

There are generally two factors which determine whether a ML model is understandable [78], i.e. the human’s understanding given through capacity, and the model’s features. Evaluating explainability is thus a result of combining these two factors. To this end, [18] describe three categories of explainability evaluation approaches.

Application-grounded Evaluation Application-grounded evaluation measures the quality of an explanation in the context of its intended task, such as whether it results in less discrimination or better error identification. The benefit lies in testing to what extent the explainability method is helpful to the user [55]. Exemplary experiments include domain expert experiments with identical or simpler application tasks. For instance, if the task is to diagnose a particular disease, the most ideal way to demonstrate the model’s workings is to have doctors perform the diagnosis. A good indication of explainability is how well they explain a decision [48].

Human-grounded Evaluation Human-grounded evaluation assesses simpler human-subject experiments while maintaining the essence of the target application. This has several benefits, especially when the goal is to test general notions of explanation quality. Also, it is less expensive and may use a bigger subject pool, as lay humans are able to participate. Preferably, this evaluation approach solely depends on the quality of the explanation, regardless of the type of explanation or the correctness of the associated prediction. Possible experiments include a binary forced choice, forward simulation and counterfactual simulation. For instance, one might ask a user to simply choose the best fitting explanation from a pool of explanations [48].

Functionally-grounded Evaluation Functionally-grounded evaluation does not demand human experiments but instead uses a formal definition of explainability as a proxy for explanation quality. Hence, it is most appropriate when a class of methods has already been evaluated, when a method is not yet mature enough, or when human-subject experiments would be unethical. The approach benefits from lower time and cost requirements, as no human-subject experiments are necessary. However, [14] argue that results from a functionally-grounded approach have low validity, as human feedback is missing and the defined proxies may not fully measure explainability.

2.4 Evaluation Metrics

With application- and human-grounded evaluations, selecting the correct evaluation metrics plays a critical role so as to correctly evaluate a method. To this end, [78] differentiate between *subjective* and *objective* metrics. Subjective metrics are surveyed during, or after a task to gather the user’s subjective response. They include trust, confidence, preference, or reasonability, and as such have been used in a variety of previous evaluations (e.g., [56, 79, 77]). Objective metrics are surveyed before, during, or after a task. They include human metrics, such as physiological and behavioral indicators, informed decision-making, task time length, or task performance. [61], for example, demonstrated that faster and more accurate decisions regularly indicate an intuitive understanding of explanations.

Functionally-grounded evaluation metrics, on the other hand, consist of various quantitative metrics to objectively assess the quality of an explanation, or more specifically whether certain explainability axioms are met [78]. Benchmarks without human intervention also fall under this category [55]. Examples contain model size [26], remove and retrain (ROAR) [30], diversity [50], sanity checks [3], or interaction strength [44].

While many quantitative metrics are proposed, a general computational benchmark across all possible explainability methods is difficult [50], as explainability is still a subjective concept where the perceived quality is user and task dependent.

2.5 Neural Network Pruning

Neural Network (NN) pruning describes the deletion/reduction of network parameters. Modern neural networks are typically over-parameterized for the task at hand, leading to extensive redundancies in the model [41]. The goal of pruning is to reduce these redundancies and with it storage and memory requirements, which ultimately helps save computational resources. While the idea of network pruning has initially been introduced in the late 1980’s [38], it is the emergence of deep learning and the consequent rise in memory and storage requirements [11], which has recently led to an increased interest in the concept. Moreover, it has been shown that a careful selection of the to-be-removed parameters does not only reduce the resource requirements of a model, but may even increase its accuracy [22, 27]. Research has shown that using NNs with a lower number of parameters from the start does not achieve the same accuracy than using a larger model and prune it retrospectively [27]. Pruning approaches may be described along five dimensions:

(1) The **selection criterion** defines how to select the parameters to be pruned. Many approaches have been proposed, e.g., based on absolute values [27], the gradients [11], the Hessian matrix of the loss function [38], or based on the L_2 norm of the network structure [29]. Network pruning can also be incorporated into the DNN’s learning procedure [33] or be formulated as its own optimization

problem [74]. Finally, random pruning often serves as a baseline and sanity check [11, 22].

(2) The **scope** determines whether the selection process is performed locally [29], where each layer is pruned separately, or globally, where all weights are considered simultaneously for the selection process. Global network pruning results in different sparsity levels in each layer, while local pruning yields a steady pruning ratio over the whole network [11].

(3) **Scheduling** defines when pruning is conducted. Most methods, e.g. [27], apply pruning after the training. The network is either pruned in one step to the desired compression rate [41], called one-shot pruning, or an iterative process of pruning and consequent training is applied [27, 23].

(4) The **pruning-structure** describes the granularity of a method, where the unstructured approach prunes single weights [38, 11], while structured pruning removes entire parts, such as kernels and filters [29], or even whole residual blocks [33]. Since the first approach produces sparse matrices of the same size as the unpruned network, dedicated hardware is necessary to accomplish practical improvements.

(5) **Fine tuning** refers to the training phase, which happens after pruning is applied. Here, recent work explores whether retraining a pruned network from scratch, using a new set of randomly initialized values, would lead to a different accuracy [41] than fine-tuning the remaining weights with their pre-pruning values [27]. To this end, the lottery ticket hypothesis proposed by [22] suggests that a pruned network can reach a higher accuracy than its unpruned equivalent when retrained from scratch using its initial (random) values.

The amount of parameters that is removed by NN pruning is measured in pruning compression rates (CPRs), where a CPR of 1 stands for the unpruned, original NN, while a CPR of 2 expresses that the final network has only half of the original parameters, a CPR of 4 that the resulting NN has only a fourth of the original NN’s parameters and so forth.

2.6 Neural Network Pruning to Increase Explainability

Previous work on leveraging NN pruning for ML explainability is scarce. For example, [35] argue that current gradient-based attribution methods produce noisy results due to the complexity of current model architectures. Yet, if one uses input-specific pruning, where only neurons with high predictive contributions are kept, the global importance information of the attribution method may be improved. Their approach called PruneGrad differs from traditional model pruning in (1) that it does not take the whole dataset into account, (2) that it does not decrease the memory footprint, and (3) that it does not increase the inference speed. It was shown that roughly 50% of neurons can be removed without any changes in the output, while excessive pruning (i.e., over 80%) also removes highly contributing neurons and thus results in significant output changes. To perform a functionally-grounded evaluation of their PruneGrad method, [35] applied the sanity checks by [3], the pixel perturbation benchmark by [59], and

the ROAR framework by [30]. Evaluation results consistently outperform other gradient-based attribution methods.

[1], on the other hand, extended previously proposed filter importance indices so as to visually apply filter pruning. Their structured algorithm prunes filters with visually redundant pattern selectivity, thereby increasing the explainability of the CNN. As a result, memory savings and smaller computational costs are reached while making the CNNs more explainable.

Other scientific contributions leverage explainability methods as a means for model pruning. For example, the work of [20] explored the suitability of datasets for certain models once they are pruned. Doing so, they showed that visualizing a sample dataset of the final convolutional layer for different pruning ratios, helps in making class separability visually understandable. Building on this, [75] were the first to use explainability theory to actually guide channel pruning.

Other works apply different model explainability methods as CNN pruning criteria, as it is a challenge to identify criteria by which the importance of parameters can be measured. [72], for example, used Layer-wise relevance propagation (LRP) [9]. Their results show that the novel LRP criterion is not only comparable to state-of-the-art but clearly outperforms previous criteria in transfer-learning scenarios. [58] utilized DeepLIFT [64] to obtain the importance of certain neurons for NN pruning and the quantification of NN weights. With this they aimed to address a broad range of pruning methods, including structured, unstructured, CNN filter, and neuron pruning.

Finally, [71] proposed an explainability-based filter pruning framework based on activation maximization [73]. By visualizing every filter with activation maximization, they found that over 50% of the filters contain either repetitive or no information at all, making them redundant or invalid. The filters were then pruned based on a filter similarity matrix, which measured color and texture similarities. While maintaining a high level of accuracy after pruning, the advantage of this method lies in also removing superfluous filters, not only the unimportant ones.

Summarizing, we may argue that NN explainability methods are far more utilized to guide NN pruning than NN pruning is utilized to support NN explainability, although previous work has shown that there is merit in the latter. The goal of our work was thus to focus on NN pruning for ML explainability and measure its suitability using human-grounded evaluation.

3 Methodology

The goal of our work was to investigate the influence of NN pruning on the explainability of CNNs. In particular, we focused on the CPR (cf. Section 2.5) as a variable to indicate the extent of NN pruning and assess its effects on perceived CNN explainability. In this sense, our methodology may be described as a three-phase experimental study, i.e., pre-study, Experiment 1, and Experiment 2. Following we first describe the technical setup we used and then provide more details on the three human-grounded experiments.

3.1 Technical Setup

Throughout the experiments, we use the VGG model proposed by [66]. Specifically, we choose VGG-16 (configuration *D*). Its structure is simple and homogeneous, consisting of 13 convolutional layers and 3 fully connected layers. Due to its depth and high number of parameters (138 million) VGG-16 provides an adequate architecture for applying NN pruning.



Fig. 3: Example images of the Imagenette dataset with their labels.

We decided to use the Imagenette¹ dataset by FastAI². Imagenette is a subset of Imagenet³, one of the largest image databases for model benchmarks and research, and consists of ten classes, namely *tench*, *English springer*, *cassette player*, *chain saw*, *church*, *French horn*, *garbage truck*, *gas pump*, *golf ball* and *parachute* [31]. Figure 3 shows one sample of each class in the dataset. We chose this dataset for two reasons. First, the smaller size of the dataset requires less computing power and overall runtimes. Second, we decided to choose a model architecture that was already pre-trained on Imagenet, allowing us to easily finetune it on Imagenette. During the experiments, the class *tench* was changed to *fish* and the class *English springer* was changed to *dog*. This change simplified the Imagenette classes, as we did not anticipate our participants to have knowledge about fish species or dog breeds.

The pre-trained VGG-16 was finetuned on Imagenette. The model reached a training accuracy of 99% and a validation accuracy of 98%. On the test-set, we reached a top-1 accuracy of 97%. Following common baseline conventions in NN pruning research (e.g [27], [23]), we applied iterative magnitude-based

¹ Online: <https://github.com/fastai/imagenette> [accessed: February 20, 2023]

² Online: <https://www.fast.ai> [accessed: February 20, 2023]

³ Online: <https://www.image-net.org> [accessed: February 20, 2023]

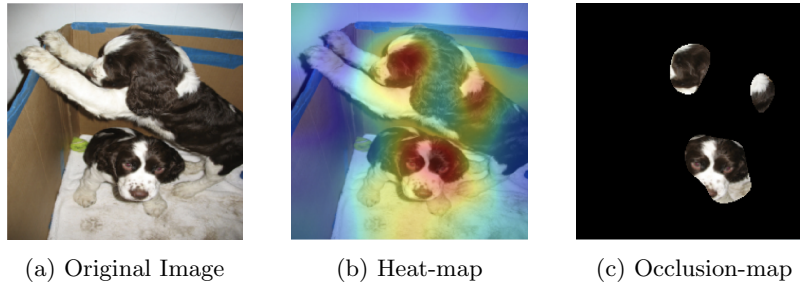


Fig. 4: An image of the class 'dog', its heat- and occlusion-map based on Grad-CAM and our calculations

weight-pruning. To implement this method, we utilized the PyTorch pruning library [51].

As convolutional layers contribute the most to the inference time of CNNs and thus, have the greatest potential for theoretical speed-ups [47], we only pruned the convolutional layers of the network. The previously trained and converged VGG-16 was then iteratively pruned for every CPR $\{2, 4, 8, 16, 32\}$. After every CPR, the model was retrained until convergence. Figure 2 (on page 3) shows the top-1 accuracy on the Imagenette test-set for every CPR, including the accuracy of the unpruned VGG-16 (= CPR 1) (in dark blue).

We opted to implement Grad-CAM, utilizing the PyTorch hooking mechanisms⁴, due to its objective qualification as an explainability-method [3] and its relevance in both, research and real-world applications. We crafted two types of images from the resulting activation-map matrices: Heat-maps and occlusion-maps. Figure 4 includes an example image with its heat-map and occlusion-map.

For the **heat-map** images, the activation-map matrix was up-sampled to the input image size of (224×224) pixels and visualized in colors from red (very important) to blue (least important). We then applied the heat-map over the original image with an opacity of $\alpha = 0.4$.

For the **occlusion-map** images the activation-map matrix was up-sampled to the input image size. Instead of colors indicating the importance, the least important 90% of the pixels are masked. These occlusion-maps are inspired by the visualizations in Grad-CAM++[15], where the idea is to display only the parts of the image that appear to be most important to the network's decision. We decided to use 90% after visual inspection of some examples with varying degrees of occlusion.

⁴ Online: https://pytorch.org/tutorials/beginner/former_torchies/nnft_tutorial.html#forward-and-backward-function-hooks [accessed: February 20, 2023]

3.2 Experimental Setup

Our research design was based on a three-phase approach, containing a pre-study and two more focused experiments. While the pre-study and the first experiment were exploring the participants’ subjective perception, the second experiment was evaluating the participants’ performance based on objective metrics, leveraging [61]’s findings that more accurate decision-making indicates better explanation.

We used Amazon’s Mechanical Turk⁵ (MTurk) platform for all experiments in order to gather sufficient data. To ensure high-quality results, only MTurk respondents with a human intelligence task approval rate greater than 90% were admitted.

In the following, we present the setups for each of these phases and rationalize their design choices.

Pre-study For the pre-study, we created heat- and occlusion-maps for the models with CPR 1, 2, and 32. CPR 1, i.e., the non-pruned model, acted as the base-line. The great distance between CPR 2 and CPR 32 provided results from two different ends of the pruning spectrum. We used 500 Imagenette test-set images – 50 of each class. All test-set images were predicted correctly by all three models. For every image and CPR, we created a heat- and an occlusion-map, resulting in three heat-maps and three occlusion-maps per image, i.e. a total of 1 500 heat-maps and 1 500 occlusion-maps. Participants were confronted with three images:

- the original image, always placed in the middle with the correctly predicted class
- a heat-map image crafted with the unpruned model, randomly placed on either the left or right side
- a heat-map image crafted by either the CPR 2 model or the CPR 32 model on the other side

The setup generated a total of 1 000 unique tasks (two for each original image). The CPR was unknown to the participants, assuring a blind-study setup. Participants were asked to select the algorithm whose predictions they believed was more reasonable, or in case both algorithms felt equally reasonable select the middle point. The same setup was used for the occlusion-map images, resulting in another 1 000 unique tasks. Exemplary setups of the pre-study can be found in Figures 13 and 14 in Appendix A.

Every of the 2 000 unique tasks was answered five times, generating a total of 10 000 answers.

Experiment 1 Lessons learned from our pre-study, that influenced the setup of Experiment 1 were: First, the CPRs do have an influence on the explainability of

⁵ Online: <https://www.mturk.com> [accessed: February 20, 2023]

the CNN, second, heat-maps seem to be more suitable than occlusion-maps for the evaluation with a subjective metric, and third, CPR 32 does not only influence the CNNs accuracy negatively (cf. Fig. 2, on page 3) but also explainability to humans⁶.

With these lessons in mind, we decided to use heat-maps only for Experiment 1. Furthermore, we decided to extend the three-point Likert-scale to a five-point Likert-scale and to disregard the model with CPR 32 in favor of models with CPR 4 and CPR 8. Figure 1 (on page 1) shows the presentation of a single task. For this experiment we decided to focus on the heat-map images, as the pre-study had shown that these images produced clearer results. Again, participants were asked to decide which of the algorithms was more reasonable in its decision-making based on the shown heat-map images. This time, participants were asked to make a more nuanced selection based on a 5-point Likert scale running from *clearly more reasonable* (cmr) to *clearly less reasonable* (clr) with *slightly more reasonable* (smr), *equally reasonable* (eq), and *slightly less reasonable* (slr) in between. We crafted 500 heat-map images for the CPRs 1, 2, 4, 8, and compared each CPR with every other CPR, resulting in 3 000 unique tasks. Every unique task was answered by 5 respondents generating a total of 15 000 answers.

Evaluation

In order to calculate an inter-coder agreements we encoded all answer possibilities with values ranging from -2 for *clearly less reasonable* to +2 for *clearly more reasonable*. Then, we used Krippendorff’s α [36] to calculate an agreement level. Additionally we report the inter-rater agreement based on the standard deviation of the respondents per task. With five respondents per task and the answers encoded as mentioned above, the standard deviation may compute to 26 different values ranging from 0 (where we have full agreement, i.e., all respondents choose the same option) to 1.9596 (where we have complete disagreement, e.g. two respondents answer with clearly more reasonable and three with clearly less reasonable). Thus, we can say that lower values indicate more agreement among respondents, while higher values translate to more disagreement. The value of $\sqrt{2}$ (i.e. one answer per option) may serve as a baseline that indicates randomness, meaning that values below $\sqrt{2}$ tend to more agreement and values above to more disagreement.

To give an intuition we sampled some of these 26 possibilities in Table 1.

As we cannot assume explainability to be transitive (i.e. even if the CPR 2 model produces more reasonable heat-maps than the CPR 1 model, and the CPR 4 model produces more reasonable heat-maps than the CPR 2 model, we cannot be sure that the CPR 4 model is more reasonable than the CPR 1 model), we observed all tasks that contain a specific CPR. Exemplary for CPR 1, we accumulated all tasks which compare CPR 1 with either CPR 2, CPR 4 or CPR 8. The mean of all respondents answers, encoded as above, then creates a metric that describes the explainability of this specific model relative to all other examined models. We define this number as a model’s *explainability index*

⁶ We report detailed results of the pre-study in Section 4.1.

cmr	smr	eq	slr	clr	
[+2, +1, 0, -1, -2]					standard deviation
[0,	0,	0,	0,	5]	0
[0,	0,	0,	1,	4]	0.4
[0,	1,	1,	2,	1]	1.0198
[0,	1,	1,	1,	2]	1.1662
[1,	1,	1,	1,	1]	$\sqrt{2}$
[1,	1,	0,	2,	1]	1.4697
[2,	0,	0,	0,	3]	1.9596

Table 1: Examples of inter-rater agreement and the corresponding standard deviations.

which allows for a direct comparison between all algorithms. Here, a higher value indicates superior explainability compared to the remaining algorithms.

Experiment 2 Experiment 2 aimed to assess the effects of different CPRs on Grad-CAM occlusion-maps and how they differ from human-understandable areas. Participants were confronted with a single occlusion-map, crafted as described in Section 3.1, i.e. based on models with CPR 1, 2, 4, 8, and 32. All occlusion-maps appeared in random order to prevent the occlusion-map of an identical image. Next to the occlusion-map, all ten Imagenette classes were listed as possible answers, as depicted in Figure 5. The respondents were instructed to choose the most suitable class for the map. In case they felt that none of the classes would fit, they were asked to choose *I don't know / None of the above*. The accuracy of the respondents' answers provides an objective evaluation metric. Note that this setup would not make much sense with heat-maps as participants would see the whole image and thus know exactly what the image displays.

In total, this resulted in 2 500 unique tasks, as 5 occlusion maps of 500 images crafted - once for every CPR. Every unique task was answered five times, generating a total of 7 500 answers.

Evaluation

To assess the inter-rater agreement we calculated Krippendorff's α [36]. As for this experiment a clear ground truth is available we were able to calculate the human-observer accuracy as the ratio of correct answers and the total amount of answers. Additionally we report the error rate as the ratio between wrong answers and the total number of answers and the ratio of images for which the respondents were indecisive. We report these numbers for each CPR in $\{1, 2, 4, 8, 32\}$ over all classes and for each individual class.

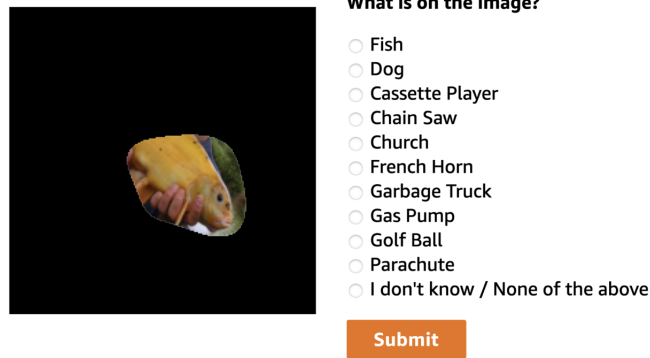


Fig. 5: Experimental Setup - Experiment 2: occlusion-map (CPR 1).

4 Results

Following we elaborate on the results of our three studies and reflect on their findings.

4.1 Pre-study

Investigating agreement levels, the pre-study setup with heat-maps achieved a Krippendorff’s α score of 0.13, while the setup with occlusion-maps achieved a score of 0.24. This indicates a rather low agreement across respondents as to which CPR for particular images appears more reasonable. The higher value for the occlusion-maps stems from the fact that here more respondents believe that both models seem equally reasonable.

	CPR 1 vs CPR 2	CPR 1 vs CPR 32
	<i>more reasonable in %*</i>	<i>(more reasonable in %*)</i>
heat-maps	46.6% vs 53.4%	52.9% vs 47.1%
occlusion-maps	45.0% vs 55.0%	54.2% vs 45.8%
	<i>equally reasonable in %</i>	<i>equally reasonable in %</i>
heat-maps	38.68%	13.16%
occlusion-maps	53.72%	26.4%

* % based on answers without “equal reasonability”

Table 2: Explainability comparison of pre-study results for different CPRs and visualization methods.

Furthermore we found that the three CPRs used (1, 2, and 32) do make a difference in explainability. The upper half of Table 2 compares the percentages of explainability between heat- and occlusion-maps. The results indicate that

	total	CPR 1	CPR 2	CPR 4	CPR 8	
Krippendorff’s α	0.086	0.0916	0.0777	0.0913	0.0904	
mean over standard deviations	1.0036	0.9904	0.9784	1.0034	1.0424	
	CPR 1 vs. CPR 2	CPR 1 vs. CPR 4	CPR 1 vs. CPR 8	CPR 2 vs. CPR 4	CPR 2 vs. CPR 8	CPR 4 vs. CPR 8
Krippendorff’s α	0.049	0.1168	0.0985	0.0806	0.0962	0.0752
mean over standard deviations	0.8873	1.0185	1.0654	0.9889	1.0588	1.0029

Table 3: Inter-rater agreement for the first experiment. The “total” column is measured over all responses, the other four columns in the top row are calculated per CPR against all other CPRs, all lower columns are calculated for the specified CPR-comparison.

the unpruned model has worse explainability than the CPR 2 model but is more explainable than the CPR 32 model.

The lower half of Table 2 presents, the percentage of respondents that chose “Both are equally reasonable”. We can see that this number is clearly higher for occlusion-maps. A higher number for “equally reasonable” indicates that NN pruning has not as much of an effect on the explainability of the occlusion-maps.

Overall, Table 2 suggests that occlusion-maps are more robust to different pruning ratios, as can be seen by the higher number of indecisive respondents, and thus not as suitable to assess the difference between different pruning ratios as heat-maps. Hence, one of the most important result from our pre-study is that considering the task of assessing explainability to humans, heat-maps are more suitable than occlusion-maps.

4.2 Experiment 1: Which Algorithm is More Reasonable?

We report the inter-rater agreement for the first experiment in Table 3. Independent of the applied CPR, Krippendorff’s α is relatively low, indicating low agreement among the respondents. As described in Section 3.2, we further report the mean over the per-task standard deviation. Over all tasks, we observe values between 0 (complete agreement) and 1.9596 (complete disagreement). Further, the mean of the standard deviation over all tasks is 1.0036, which is clearly below $\sqrt{2}$ (the standard deviation of a uniform distribution), indicating a certain level of agreement among the respondents.

Figure 6 depicts all per comparison results. The upper three graphs show the accumulated answers for the comparisons of the unpruned model with models pruned with CPR 2, 4, and 8, respectively. We observe that the proportion of participants rating both algorithms equally reasonable declines when increasing the CPR. Further, the lower three graphs in Figure 6 show the accumulated answers for the tasks in which two pruned models are compared. Apart from the change in the amount of respondents that find both algorithms equally reason-

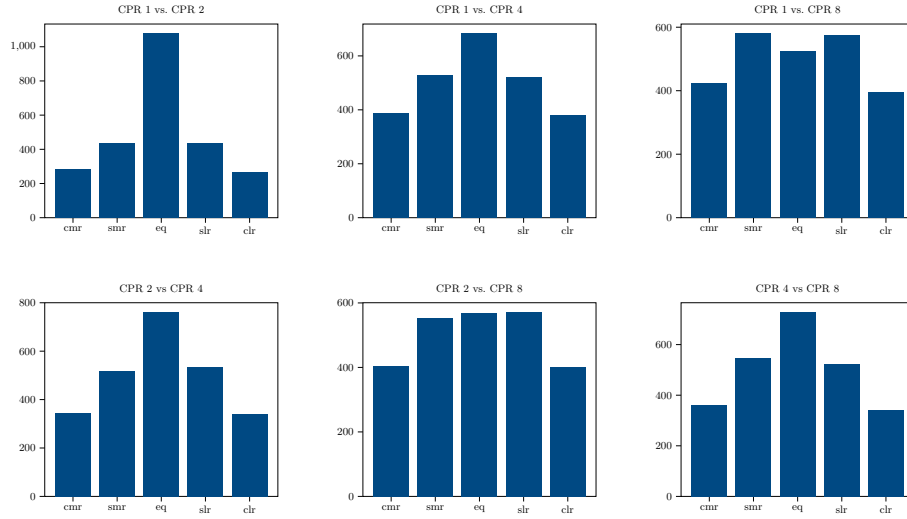


Fig. 6: The distribution of participants’ answers for each model comparison. The higher CPR is always compared to the lower CPR. (Mind the different y-axes.)

able, visually no clear trends are detectable. However, in Table 4 we report the mean of the respective encoded answers. Values above 0 indicate that the first-mentioned algorithm produces more explainable heat-maps while values below 0 indicate the opposite. One can see that in total, pruning with CPRs 2, 4, and 8 (upper three lines) seem to help the explainability to human raters. Transitivity, however, is not given. When considering the baseline experiments comparing the unpruned with the pruned models, we would expect the CPR 8 model to produce better explainable heat-maps than the CPR 2 model. However, when comparing the respective heat-maps directly, participants perceived the heat-maps of the CPR 2 model to be more reasonable than both, the CPR 4 and CPR 8 model (as can be seen in lines 4 and 5 of Table 4).

Table 5 illustrates the explainability index as described in Section 3.2, that is the explainability of heat-maps produced with every CPR compared to every other CPR. By this metric, measured over all tested images, heat-maps produced with the CPR 8 model explain the model’s decision most reasonably. Interestingly, the CPR 2 and the CPR 4 model both produce more reasonable explanations than the unpruned model. The orange line in Figure 2 (on p. 3) and Figure 7 illustrate these findings visually.

4.3 Experiment 2: What is on the Image?

We assess the inter-rater agreement for this experiment with Krippendorff’s α . Table 6 shows the α -values over all answers, and for the specific CPRs. The overall α of 0.76 indicates a reasonable high agreement among the respondents.

Algorithm 1	Algorithm 2	Mean
CPR 1	CPR 2	-0.0128
CPR 1	CPR 4	-0.0104
CPR 1	CPR 8	-0.0272
CPR 2	CPR 4	0.0036
CPR 2	CPR 8	0.0048
CPR 4	CPR 8	-0.0232

Table 4: Mean over all answers for the specific comparisons with answers encoded from -2 (Algorithm 1 is clearly less reasonable) to +2 (Algorithm 1 is clearly more reasonable).

Algorithm	Explainability Index
CPR 1	-0.0168
CPR 2	0.0071
CPR 4	-0.0055
CPR 8	0.0152

Table 5: Explainability index for all models

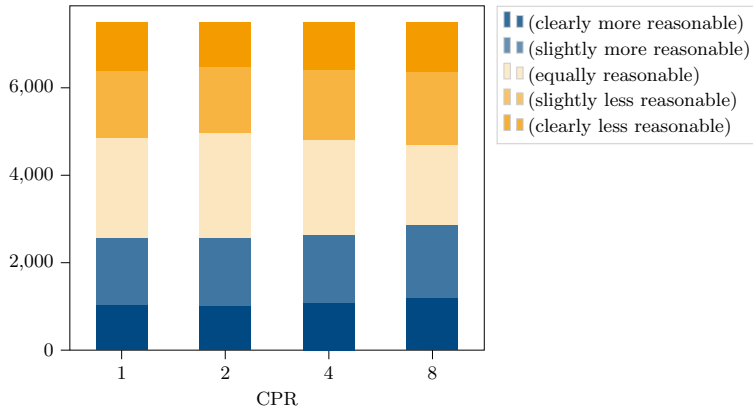


Fig. 7: The collected results of Experiment 1 for all CPRs.

Interestingly, the inter-rater agreement is higher for the unpruned (≈ 0.80) and CPR 2 pruned (≈ 0.79) models and declines for higher pruning ratios (≈ 0.74).

Table 7 shows the overall results of the second experiment. Mind that all values refer to the human-respondents’ performance. We observe that the participants achieve a slightly higher accuracy for the occlusion-maps produced with the CPR 2 model (86.40%) over those produced with the unpruned model (85.84%). For higher pruning rates, the human-rater accuracy declined by 4.32% (CPR 4) to 5.2% (CPR 8). The human error rate is relatively stable, with the lowest value for the unpruned model (4.36%) and the highest values for CPR 4 and CPR 8 (5.36% each). For the ratio of answers in which the respondents have chosen the option *I don’t know / None of the above* we observe a marginal decline from CPR 1 (9.8%) to CPR 2 (8.96%) and a subsequent rise up to 14.2% for CPR 32. Higher indecisiveness of the respondents indicates lower explainability due to indecipherable occlusion-maps. However, indecisiveness might be preferable over a wrong answer since it would be better for an explanation-map

Krippendorff's α 's	
CPR 1	0.799268
CPR 2	0.790250
CPR 4	0.744596
CPR 8	0.738209
CPR 32	0.744790
total	0.763540

Table 6: Krippendorff's α 's per CPR in Experiment 2.

	Accuracy	Error-rate	Indecisive
CPR 1	85.84%	4.36%	9.80%
CPR 2	86.40%	4.64%	8.96%
CPR 4	82.08%	5.36%	12.56%
CPR 8	81.20%	5.36%	13.44%
CPR 32	81.32%	4.48%	14.20%

Table 7: Overall results of Experiment 2.

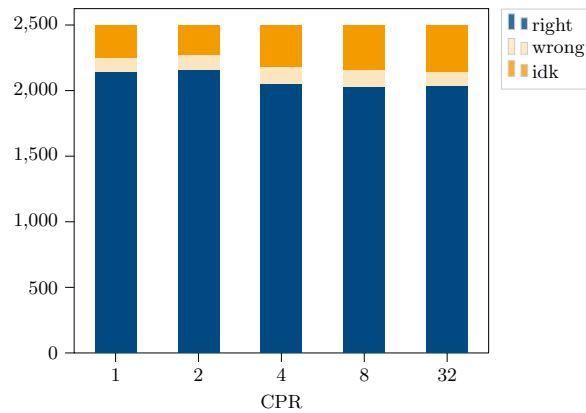


Fig. 8: Respondents' answers in Experiment 2 for all CPRs.

to explain nothing, rather than explaining the wrong class. The light blue line in Figure 2 (on page 3) shows the human rater accuracy and Figure 8 illustrate the distribution of respondents' answers visually.

The human-rater performance differs vastly between the classes. Table 8 displays the accuracies for all ten classes dependent on the CPR of the used model. For occlusion-maps produced with the unpruned model, human-rater accuracy ranges from 66% (chainsaw) to 95.6% (golfball). Interestingly, the impact of neural network pruning on the reasonability of the produced occlusion-maps is also dependent on the class. For some classes, the human-rater accuracy declines sharply when the underlying model is pruned. As an example, the human-rater performance for the class 'parachute' is high (88%) with the unpruned model, but heavily declines for CPR 2 (80.4%) and CPR 4 (71.2%). On the other hand, for the class 'dog' respondents achieved the lowest accuracy (90%) for occlusion-maps produced with the unpruned model, while they were able to correctly classify the occlusion-maps produced with the CPR 8 model in more than 97% of the cases.

A similar observation can be made when looking at the ratio of occlusion-maps for which the respondents choose the option *None of the above / I don't*

class	Human rater accuracies					Human rater error rates				
	CPR 1	CPR 2	CPR 4	CPR 8	CPR 32	CPR 1	CPR 2	CPR 4	CPR 8	CPR 32
fish	91.2%	92.4 %	84.0 %	77.6 %	76.4 %	2.0%	0.4%	2.4%	4.0%	6.0%
dog	90.0%	95.2 %	95.6 %	97.2 %	96.0 %	1.2%	0.8%	2.0%	0.8%	0.8%
cassetteplayer	79.6%	82.4 %	73.2 %	71.6 %	77.6 %	7.2%	5.6%	10.8%	10.8%	8.4%
chainsaw	66.0%	66.0 %	58.8 %	56.4 %	52.4 %	11.6%	12.0%	14.8%	14.4%	12.0%
church	85.2%	92.4 %	90.8 %	89.6 %	88.4 %	2.0%	4.0%	1.6%	0.8%	1.6%
frenchhorn	94.0%	94.0 %	86.8 %	89.6 %	94.4 %	2.0%	2.8%	6.0%	4.4%	0.4%
garbagetruck	86.0%	88.0 %	86.4 %	84.8 %	84.4 %	6.8%	6.8%	6.0%	5.6%	3.6%
gaspump	82.8%	76.0 %	77.6 %	77.2 %	78.8 %	5.6%	9.2%	8.0%	6.8%	8.4%
golfball	95.6%	97.2 %	96.4 %	91.6 %	88.0 %	2.0%	1.2%	0.8%	2.4%	2.0%
parachute	88.0%	80.4 %	71.2 %	76.4 %	76.8%	3.2%	3.6%	1.2%	3.6%	1.6%
total	85.85%	86.40%	82.08%	81.20 %	81.32 %	4.36%	4.64%	5.36%	5.36%	4.48%

Table 8: Accuracies and error rates per class for human raters in Experiment 2. Maximum, resp. minimum are highlighted in bold face.

know. For the class ‘parachute’ the number of indecisive respondents almost doubled when comparing occlusion-maps from the CPR 1 (8.8%) and the CPR 2 (16.0%) model and rises even over 20% for the CPR 4, CPR 8, and CPR 32 model. Reversely, for the class ‘church’ indecisiveness was the highest for the CPR 1 model (12.8%) while the CPR 2 model produces the lowest value with 3.6%. We include the full table for the respondents’ indecisiveness in Appendix C.

Error rates are relatively stable among the classes and the various models, as is visible in the right half of Table 8. Respondents misclassified occlusion-maps of the class ‘chainsaw’ most often (11.6%) and pruning slightly increases the error-rate. For the class ‘cassette player’, another class with a comparatively low human-rater accuracy (see Table 8) and a higher error rate of 7.2%, mild pruning (CPR 2) decreases the error rate by 1.6% to 5.6%, while more extensive pruning increases the error rate to 10.8% (CPR 4 and CPR 8) and 8.4% (CPR 32) respectively.

The specific errors between the classes are visualized with confusion matrices in Figure 9. We observe higher error rates for occlusion-maps of images containing chainsaws and garbage trucks. This holds true for CPR 1 and CPR 2 and is also visible for higher CPRs. We provide the respective confusion matrices in Appendix C. Figure 10 illustrates the case in which fewer misclassifications occurred for the occlusion-map produced by the pruned model.

5 Limitations

We measured only low reliability scores for Krippendorff’s α for the pre-study and the first experiment. We believe that these scores are caused by the following: As pointed out in [57], the concept of explainability is subjective and domain-specific. Therefore, comparing the reasonability of two algorithms might be subjective to every respondent, especially when the two heat- or occlusion-maps do not show significant differences. This may lead to different perceptions

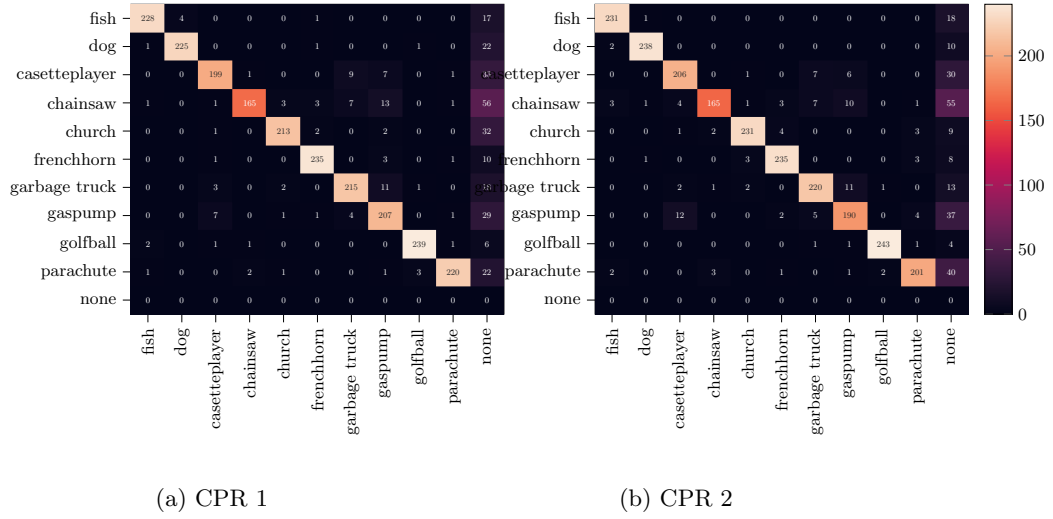


Fig. 9: Confusion matrices of the human ratings from Experiment 2 for all ten classes and CPRs 1 (Subfigure (a)) and 2 (Subfigure (b)). Darker values indicate lower numbers, lighter values indicate higher numbers. The diagonals display correct classifications, while the right-most column shows the number of ‘I don’t know / None of the above’. Confusion matrices of CPR 4, 8, and 32 can be found in Appendix C.

of the visualizations that differ among the respondents. It may further explain why the scores for Krippendorff’s α were higher in the pre-study, where we used a three-point Likert-scale, than in Experiment 1, where we used a five-point Likert-scale.

Looking at specific samples might help in understanding how complete agreement or complete disagreement might emerge. Subfigure 11a illustrates one example in which all respondents agreed on algorithm 1 to be clearly more reasonable. While the right heat-map highlights some parts on the right of the ball, the left heat-map covers the whole ball. Both heat-maps assign less importance to the print in the middle of the ball. Additionally, the heat-map on the right highlights the tee more concisely. Conversely, Subfigure 11b illustrates the case of complete disagreement, i.e. three respondents chose algorithm 1 to be clearly more reasonable, two respondents chose algorithm 2 to be clearly more reasonable. The model on the left seems to take more details into account. The participants’ degree of familiarity with the subject might be an influencing factor regarding which algorithm appears to be more reasonable.

In experiment 2, we report a rather high reliability score. In comparison to the subjectiveness of perceived explainability, experiment 2 proposes an objective measure with clear ground truth, as an image always includes one of the ten

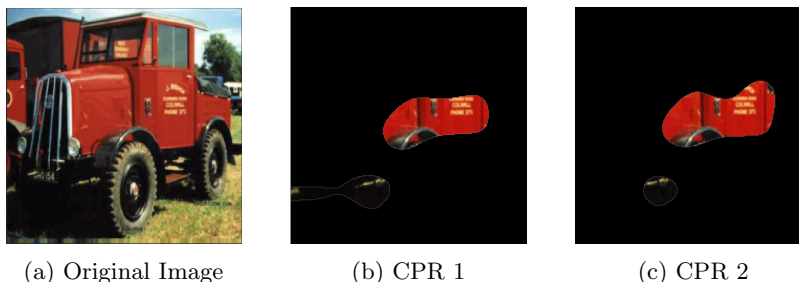


Fig. 10: The original image and occlusion-maps produced by the CPR 1 and CPR 2 models of the class 'garbage truck'. 3/5 respondents misclassified the CPR 1 occlusion-maps as a gaspump, while only 2/5 respondents misclassified the CPR 2 model as a gaspump.

Imagenette classes. If the respondents were not able to recognize the image class, they had the chance to choose 'I don't know / None of the above'.

Figure 12 shows the occlusion-maps for all five CPRs. For this sample, inter-rater agreement was reasonably high. Respondents who did not choose the correct answer all selected 'I don't know / None of the above'. Looking at the occlusion-maps, we observe that the CPR 1, CPR 8, and CPR 32 models base their prediction more on latent features of the image such as the pose of the human and the presence of a tree, while the CPR 2 and particularly the CPR 4 model base their decision on the object in question, a chainsaw, itself. Hence, it does not seem surprising that humans struggle to classify these samples correctly.

6 Future Work

Directions for future work, identified through our analyses, include the extension of the five-point Likert-scale to a seven-point Likert-scale and an experimental setup with more raters per task, maybe at the cost of a lower number of images. Carefully selecting these images, for example, by some kind of image complexity measure, would furthermore shed light on the open question about the relation between image complexity and explainability. Additionally, we restricted our setup to one explainability method and one pruning method, while there is a lot of ongoing work in each of these areas.

Besides these direct extensions of our experiments, there are several dimensions in which our work can be diversified to reach more reliable results especially in regards to generalizability. First and foremost, the generalization to other CNN architectures such as ResNets [28], Inception [68] or EfficientNets [69] should be examined. Given that we choose an explainability method that has been shown to be applicable to all CNNs, the open question is not if our methodology is applicable but rather if the results obtained for VGG-16 in this work also hold true for other CNN architectures, and subsequently also for the



(a) Heat-maps produced with the CPR 4 model on the left and the CPR 8 model on the right. All participants marked algorithm 1 to be clearly more reasonable.



(b) Heat-maps produced with the CPR 4 model on the left and the unpruned model on the right. Three participants marked algorithm 1 as clearly more reasonable, while two participants marked algorithm 2 as clearly more reasonable.

Fig. 11: Samples from Experiment 1 that yield complete agreement and complete disagreement among the human raters

novel class of transformer-based computer vision architectures, such as Swin [40] and Vision Transformers [19].

Then, related to our chosen architecture, we also examined only a single task, i.e., image classification, and it definitely would be interesting and probably more challenging to extend the experimental setup to other tasks such as object detection, image segmentation, or even image captioning. Furthermore, one could also check the validity of our results for other data sets.

Also, the extent of the occlusion in our occlusion-maps might be evaluated further. We decided to use 90% by visual examination of some examples and leave investigations as to how occlusion-maps perform which e.g. hide 85% or 95% to future work.

Finally, it might be worthy to examine the impact of NN pruning on the internal mechanisms of GradCAM (e.g. in the used activation maps) and how these changes are reflected in our human-grounded experiment results.

Exploring each of these dimensions is a valuable direction for future work and given that we carefully selected our setup, we are positive that similar setups will result in similar sweet spots.

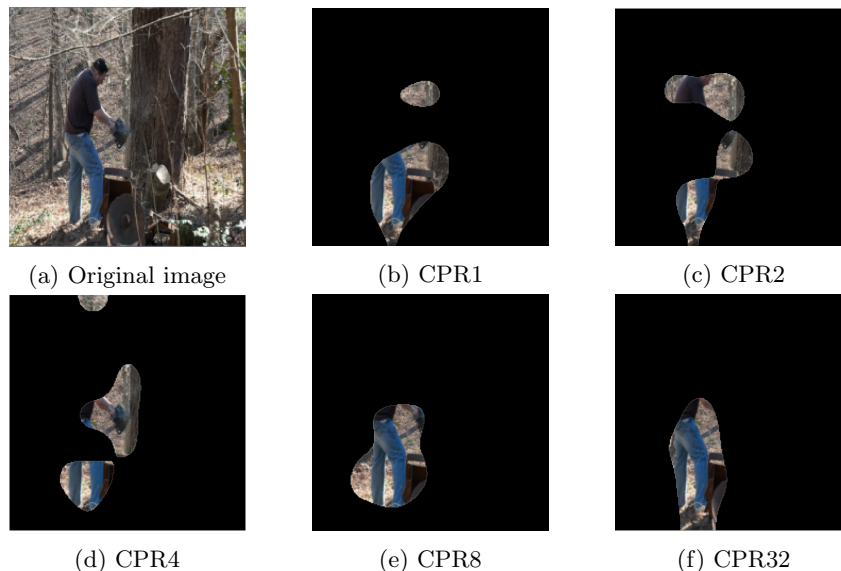


Fig. 12: The original image and occlusion-maps for one sample of the class chainsaw. Human rater accuracies are 1/5 for CPR 1, 4/5 for CPR 2, 5/5 for CPR 4, and 0/5 for CPR 8 and CPR 32.

7 Conclusion

Our results suggest that there exists a sweet spot of mild pruning, that helps explainability without hurting human decision accuracy. This might not come as a surprise as a lower number of (important) parameters seems to intuitively go along with higher explainability. But, our experiments also showed that for explainability research we always have to cover both, the subjective and the objective aspects. We did so by covering the subjective aspect in Experiment 1, which indicates that a CPR of 8 produces the best explanations. Taking the objective measure of human decision accuracy in Experiment 2 into account, however, we see that all CPRs above 2 have a negative influence on the accuracy of the participants. Additionally, it is common knowledge in the machine learning community and can be clearly seen in Figure 2 (on p. 3) that mild pruning also increases the accuracy of the underlying DNN [27]. We can even go one step further and have a look at the area of *adversarial machine learning*, which is concerned with the security of machine learning algorithms. Results from here [45], also suggest that mild pruning increases the robustness of the classifiers against malicious adversaries.

Combining our results on NN pruning and explainability with these results from machine learning and adversarial machine learning thus suggests that NN pruning might be a “jack of all trades”, which decreases complexity, computa-

tion time, power consumption while at the same time increasing explainability, accuracy, and security. So, sometimes less indeed seems to be more.

References

1. Abbasi-Asl, R., Yu, B.: Interpreting convolutional neural networks through compression. arXiv preprint arXiv:1711.02329 (2017)
2. Adadi, A., Berrada, M.: Peeking inside the black-box: a survey on explainable artificial intelligence (xai). *IEEE access* **6**, 52138–52160 (2018)
3. Adebayo, J., Gilmer, J., Muelly, M., Goodfellow, I., Hardt, M., Kim, B.: Sanity checks for saliency maps. arXiv preprint arXiv:1810.03292 (2018)
4. Alazab, M., Tang, M.: *Deep learning applications for cyber security*. Springer (2019)
5. Ali, H.M., Kaiser, M.S., Mahmud, M.: Application of convolutional neural network in segmenting brain regions from mri data. In: *International Conference on Brain Informatics*. pp. 136–146. Springer (2019)
6. Ancona, M., Ceolini, E., Öztireli, C., Gross, M.: Towards better understanding of gradient-based attribution methods for deep neural networks. arXiv preprint arXiv:1711.06104 (2017)
7. Angelov, P., Soares, E.: Towards explainable deep neural networks (xdnn). *Neural Networks* **130**, 185–194 (2020)
8. Arrieta, A.B., Díaz-Rodríguez, N., Del Ser, J., Bennetot, A., Tabik, S., Barbado, A., García, S., Gil-López, S., Molina, D., Benjamins, R., et al.: Explainable artificial intelligence (xai): Concepts, taxonomies, opportunities and challenges toward responsible ai. *Information Fusion* **58**, 82–115 (2020)
9. Bach, S., Binder, A., Montavon, G., Klauschen, F., Müller, K.R., Samek, W.: On pixel-wise explanations for non-linear classifier decisions by layer-wise relevance propagation. *PloS one* **10**(7), e0130140 (2015)
10. Bengio, Y., Courville, A.C., Vincent, P.: Unsupervised feature learning and deep learning: A review and new perspectives. *CoRR* **abs/1206.5538** (2012), <http://arxiv.org/abs/1206.5538>
11. Blalock, D., Ortiz, J.J.G., Frankle, J., Gutttag, J.: What is the state of neural network pruning? arXiv preprint arXiv:2003.03033 (2020)
12. Burkart, N., Huber, M.F.: A survey on the explainability of supervised machine learning. *Journal of Artificial Intelligence Research* **70**, 245–317 (2021)
13. Cabitza, F., Campagner, A., Ciucci, D.: New frontiers in explainable ai: understanding the gi to interpret the go. In: *International Cross-Domain Conference for Machine Learning and Knowledge Extraction*. pp. 27–47. Springer (2019)
14. Carvalho, D.V., Pereira, E.M., Cardoso, J.S.: Machine learning interpretability: A survey on methods and metrics. *Electronics* **8**(8), 832 (2019)
15. Chattopadhyay, A., Sarkar, A., Howlader, P., Balasubramanian, V.N.: Grad-cam++: Generalized gradient-based visual explanations for deep convolutional networks. 2018 IEEE Winter Conference on Applications of Computer Vision (WACV) (Mar 2018). <https://doi.org/10.1109/wacv.2018.00097>, <http://dx.doi.org/10.1109/WACV.2018.00097>
16. Cheng, L., Varshney, K.R., Liu, H.: Socially responsible AI algorithms: Issues, purposes, and challenges. *Journal of Artificial Intelligence Research* **71**, 1137–1181 (2021)

17. Dey, S., Bacellar, G.C., Chandrappa, M.B., Kulkarni, R.: Covid-19 chest x-ray image classification using deep learning. medRxiv (2021)
18. Doshi-Velez, F., Kim, B.: Towards a rigorous science of interpretable machine learning. arXiv preprint arXiv:1702.08608 (2017)
19. Dosovitskiy, A., Beyer, L., Kolesnikov, A., Weissenborn, D., Zhai, X., Unterthiner, T., Dehghani, M., Minderer, M., Heigold, G., Gelly, S., Uszkoreit, J., Houlsby, N.: An image is worth 16x16 words: Transformers for image recognition at scale. ArXiv **abs/2010.11929** (2021)
20. Dotter, M., Ward, C.M.: Visualizing compression of deep learning models for classification. In: 2018 IEEE Applied Imagery Pattern Recognition Workshop (AIPR). pp. 1–8. IEEE (2018)
21. Du, M., Liu, N., Hu, X.: Techniques for interpretable machine learning. Communications of the ACM **63**(1), 68–77 (2019)
22. Frankle, J., Carbin, M.: The lottery ticket hypothesis: Finding sparse, trainable neural networks. arXiv preprint arXiv:1803.03635 (2018)
23. Gale, T., Elsen, E., Hooker, S.: The state of sparsity in deep neural networks. arXiv preprint arXiv:1902.09574 (2019)
24. Gilpin, L.H., Bau, D., Yuan, B.Z., Bajwa, A., Specter, M., Kagal, L.: Explaining explanations: An overview of interpretability of machine learning. In: 2018 IEEE 5th International Conference on data science and advanced analytics (DSAA). pp. 80–89. IEEE (2018)
25. Goodman, B., Flaxman, S.: European union regulations on algorithmic decision-making and a “right to explanation”. AI magazine **38**(3), 50–57 (2017)
26. Guidotti, R., Monreale, A., Ruggieri, S., Turini, F., Giannotti, F., Pedreschi, D.: A survey of methods for explaining black box models. ACM computing surveys (CSUR) **51**(5), 1–42 (2018)
27. Han, S., Pool, J., Tran, J., Dally, W.J.: Learning both weights and connections for efficient neural networks. arXiv preprint arXiv:1506.02626 (2015)
28. He, K., Zhang, X., Ren, S., Sun, J.: Deep residual learning for image recognition. In: Proceedings of the IEEE conference on computer vision and pattern recognition. pp. 770–778 (2016)
29. He, Y., Kang, G., Dong, X., Fu, Y., Yang, Y.: Soft filter pruning for accelerating deep convolutional neural networks. arXiv preprint arXiv:1808.06866 (2018)
30. Hooker, S., Erhan, D., Kindermans, P.J., Kim, B.: A benchmark for interpretability methods in deep neural networks. arXiv preprint arXiv:1806.10758 (2018)
31. Howard, J.: Imagenette (2019), <https://github.com/fastai/imagenette/>
32. Huang, J., Chai, J., Cho, S.: Deep learning in finance and banking: A literature review and classification. Frontiers of Business Research in China **14**, 1–24 (2020)
33. Huang, Z., Wang, N.: Data-driven sparse structure selection for deep neural networks. In: Proceedings of the European conference on computer vision (ECCV). pp. 304–320 (2018)
34. Ker, J., Wang, L., Rao, J., Lim, T.: Deep learning applications in medical image analysis. Ieee Access **6**, 9375–9389 (2017)
35. Khakzar, A., Baselizadeh, S., Khanduja, S., Rupprecht, C., Kim, S.T., Navab, N.: Improving feature attribution through input-specific network pruning. arXiv preprint arXiv:1911.11081 (2019)
36. Krippendorff, K.: Computing krippendorff’s alpha-reliability (2011), retrieved from: https://repository.upenn.edu/asc_papers/43 [accessed: February 20, 2023]

37. Kulesza, T., Stumpf, S., Burnett, M., Yang, S., Kwan, I., Wong, W.K.: Too much, too little, or just right? ways explanations impact end users' mental models. In: 2013 IEEE Symposium on visual languages and human centric computing. pp. 3–10. IEEE (2013)
38. LeCun, Y., Denker, J., Solla, S.: Optimal brain damage. *Advances in Neural Information Processing Systems (NIPS)* **2** (1989)
39. Lipton, Z.C.: The mythos of model interpretability: In machine learning, the concept of interpretability is both important and slippery. *Queue* **16**(3), 31–57 (2018)
40. Liu, Z., Lin, Y., Cao, Y., Hu, H., Wei, Y., Zhang, Z., Lin, S., Guo, B.: Swin transformer: Hierarchical vision transformer using shifted windows. In: *International Conference on Computer Vision (ICCV)* (2021)
41. Liu, Z., Sun, M., Zhou, T., Huang, G., Darrell, T.: Rethinking the value of network pruning. *arXiv preprint arXiv:1810.05270* (2018)
42. Lundberg, S.M., Lee, S.I.: A unified approach to interpreting model predictions. In: *Proceedings of the 31st international conference on neural information processing systems*. pp. 4768–4777 (2017)
43. Mahendran, A., Vedaldi, A.: Visualizing deep convolutional neural networks using natural pre-images. *CoRR abs/1512.02017* (2015), <http://arxiv.org/abs/1512.02017>
44. Markus, A.F., Kors, J.A., Rijnbeek, P.R.: The role of explainability in creating trustworthy artificial intelligence for health care: a comprehensive survey of the terminology, design choices, and evaluation strategies. *Journal of Biomedical Informatics* , 103655 (2021)
45. Merkle, F., Samsinger, M., Schöttle, P.: Pruning in the face of adversaries. In: *The 21st International Conference on Image Analysis and Processing (ICIAP)* (2022)
46. Miller, T.: Explanation in artificial intelligence: Insights from the social sciences. *Artificial intelligence* **267**, 1–38 (2019)
47. Molchanov, P., Tyree, S., Karras, T., Aila, T., Kautz, J.: Pruning convolutional neural networks for resource efficient inference. In: *5th International Conference on Learning Representations, ICLR 2017, Toulon, France, April 24-26, 2017, Conference Track Proceedings*. OpenReview.net (2017), <https://openreview.net/forum?id=SJGCiw5gl>
48. Molnar, C.: *Interpretable Machine Learning* (2019), <https://christophm.github.io/interpretable-ml-book/>
49. Molnar, C., Casalicchio, G., Bischl, B.: Interpretable machine learning—a brief history, state-of-the-art and challenges. In: *Joint European Conference on Machine Learning and Knowledge Discovery in Databases*. pp. 417–431. Springer (2020)
50. Nguyen, A.p., Martínez, M.R.: On quantitative aspects of model interpretability. *arXiv preprint arXiv:2007.07584* (2020)
51. Paganini, M., Forde, J.: Streamlining tensor and network pruning in pytorch. *arXiv preprint arXiv:2004.13770* (2020)
52. Pathak, A.R., Pandey, M., Rautaray, S.: Application of deep learning for object detection. *Procedia computer science* **132**, 1706–1717 (2018)
53. Ploder, C., Weber, D., Bernsteiner, R., Schlögl, S.: Knowledge gain in production planning and execution systems. In: Uden, L., Ting, I.H., Wang, K. (eds.) *Knowledge Management in Organizations*. pp. 138–146. Springer International Publishing, Cham (2021)
54. Ras, G., van Gerven, M., Haselager, P.: Explanation methods in deep learning: Users, values, concerns and challenges. In: *Explainable and interpretable models in computer vision and machine learning*, pp. 19–36. Springer (2018)

55. Ras, G., Xie, N., van Gerven, M., Doran, D.: Explainable deep learning: A field guide for the uninitiated. *Journal of Artificial Intelligence Research* **73**, 329–397 (2022)
56. Ribeiro, M.T., Singh, S., Guestrin, C.: ” why should i trust you?” explaining the predictions of any classifier. In: *Proceedings of the 22nd ACM SIGKDD international conference on knowledge discovery and data mining*. pp. 1135–1144 (2016)
57. Rudin, C.: Please stop explaining black box models for high stakes decisions. *stat* **1050**, 26 (2018)
58. Sabih, M., Hannig, F., Teich, J.: Utilizing explainable ai for quantization and pruning of deep neural networks. *arXiv preprint arXiv:2008.09072* (2020)
59. Samek, W., Binder, A., Montavon, G., Lapuschkin, S., Müller, K.R.: Evaluating the visualization of what a deep neural network has learned. *IEEE transactions on neural networks and learning systems* **28**(11), 2660–2673 (2016)
60. Samek, W., Montavon, G., Vedaldi, A., Hansen, L.K., Müller, K.R.: *Explainable AI: interpreting, explaining and visualizing deep learning*, vol. 11700. Springer Nature (2019)
61. Schmidt, P., Biessmann, F.: Quantifying interpretability and trust in machine learning systems. *arXiv preprint arXiv:1901.08558* (2019)
62. Selvaraju, R.R., Cogswell, M., Das, A., Vedantam, R., Parikh, D., Batra, D.: Grad-cam: Visual explanations from deep networks via gradient-based localization. In: *Proceedings of the IEEE international conference on computer vision*. pp. 618–626 (2017)
63. Selvaraju, R.R., Cogswell, M., Das, A., Vedantam, R., Parikh, D., Batra, D.: Grad-CAM: Visual Explanations from Deep Networks via Gradient-Based Localization. *International Journal of Computer Vision* **128**(2), 336–359 (2020). <https://doi.org/10.1007/s11263-019-01228-7>, <https://doi.org/10.1007/s11263-019-01228-7>
64. Shrikumar, A., Greenside, P., Kundaje, A.: Learning important features through propagating activation differences. In: *International Conference on Machine Learning*. pp. 3145–3153. PMLR (2017)
65. Simonyan, K., Vedaldi, A., Zisserman, A.: Deep inside convolutional networks: Visualising image classification models and saliency maps. In: Bengio, Y., LeCun, Y. (eds.) *2nd International Conference on Learning Representations, ICLR* (2014)
66. Simonyan, K., Zisserman, A.: Very deep convolutional networks for large-scale image recognition. *arXiv preprint arXiv:1409.1556* (2014)
67. Sundararajan, M., Taly, A., Yan, Q.: Axiomatic attribution for deep networks. In: *International Conference on Machine Learning*. pp. 3319–3328. PMLR (2017)
68. Szegedy, C., Liu, W., Jia, Y., Sermanet, P., Reed, S., Anguelov, D., Erhan, D., Vanhoucke, V., Rabinovich, A.: Going deeper with convolutions. In: *Proceedings of the IEEE conference on computer vision and pattern recognition*. pp. 1–9 (2015)
69. Tan, M., Le, Q.: Efficientnet: Rethinking model scaling for convolutional neural networks. In: *International Conference on Machine Learning*. pp. 6105–6114. PMLR (2019)
70. Tjoa, E., Guan, C.: A survey on explainable artificial intelligence (xai): Toward medical xai. *IEEE Transactions on Neural Networks and Learning Systems* (2020)
71. Yao, K., Cao, F., Leung, Y., Liang, J.: Deep neural network compression through interpretability-based filter pruning. *Pattern Recognition* , 108056 (2021)
72. Yeom, S.K., Seegerer, P., Lapuschkin, S., Binder, A., Wiedemann, S., Müller, K.R., Samek, W.: Pruning by explaining: A novel criterion for deep neural network pruning. *Pattern Recognition* **115**, 107899 (2021)

73. Zeiler, M.D., Fergus, R.: Visualizing and understanding convolutional networks. In: European conference on computer vision. pp. 818–833. Springer (2014)
74. Zhang, T., Ye, S., Zhang, K., Tang, J., Wen, W., Fardad, M., Wang, Y.: A systematic dnn weight pruning framework using alternating direction method of multipliers. In: Proceedings of the European Conference on Computer Vision (ECCV). pp. 184–199 (2018)
75. Zhang, Y., Lin, M., Lin, C.W., Chen, J., Huang, F., Wu, Y., Tian, Y., Ji, R.: Channel pruning in a white box for efficient image classification (2021)
76. Zhou, B., Khosla, A., Lapedriza, A., Oliva, A., Torralba, A.: Learning deep features for discriminative localization. In: Proceedings of the IEEE conference on computer vision and pattern recognition. pp. 2921–2929 (2016)
77. Zhou, J., Arshad, S.Z., Yu, K., Chen, F.: Correlation for user confidence in predictive decision making. In: Proceedings of the 28th Australian Conference on Computer-Human Interaction. pp. 252–256 (2016)
78. Zhou, J., Gandomi, A.H., Chen, F., Holzinger, A.: Evaluating the quality of machine learning explanations: A survey on methods and metrics. *Electronics* **10**(5), 593 (2021)
79. Zhou, J., Li, Z., Hu, H., Yu, K., Chen, F., Li, Z., Wang, Y.: Effects of influence on user trust in predictive decision making. In: Extended Abstracts of the 2019 CHI Conference on Human Factors in Computing Systems. pp. 1–6 (2019)

A Additional Material from the Pre-study

Figures 13 and 14 demonstrate the experimental setup of the pre-study.

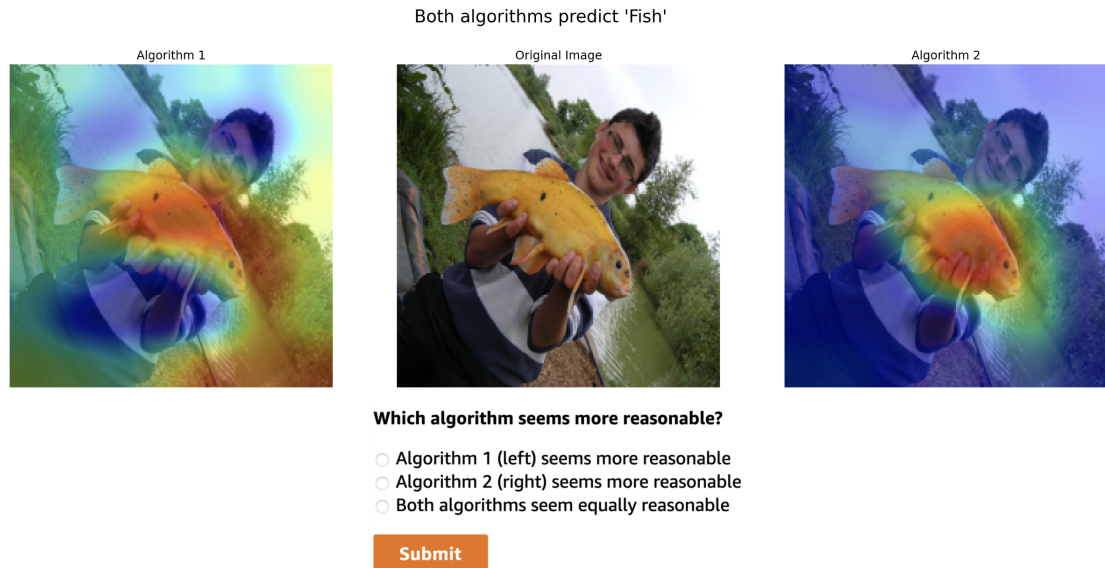


Fig. 13: Experimental Pre-study setup with heat-maps CPR 32 (left) vs. CPR 1 (right).

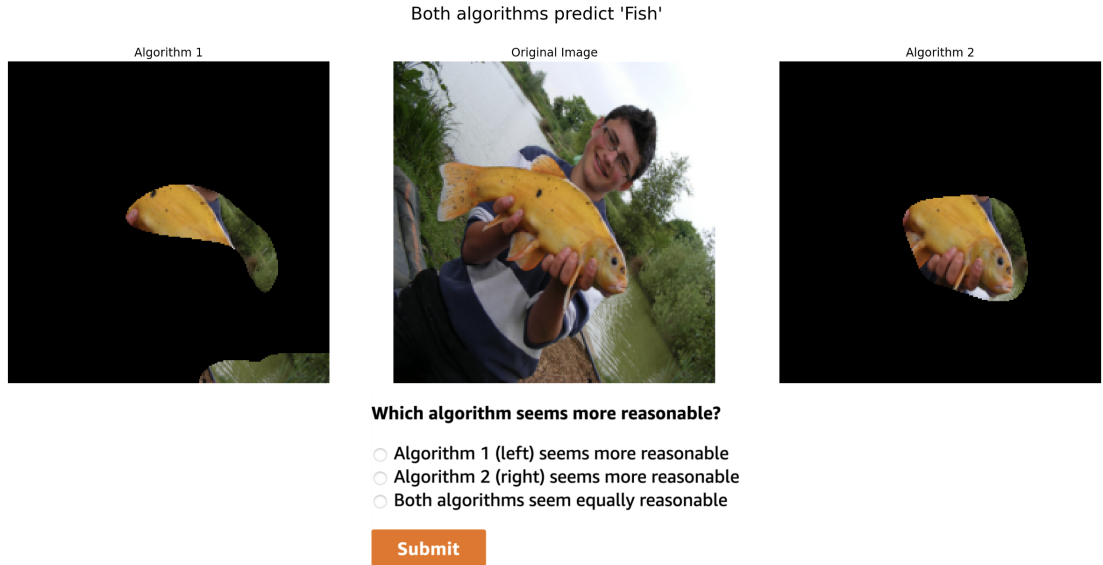


Fig. 14: Experimental Pre-study setup with occlusion-maps CPR 32 (left) vs. CPR 1 (right).

B Additional Material from Experiment 1

Figure 15 demonstrates the distribution of the answers for each CPR in experiment 1. The change in distribution is clearly visible between the CPRs.

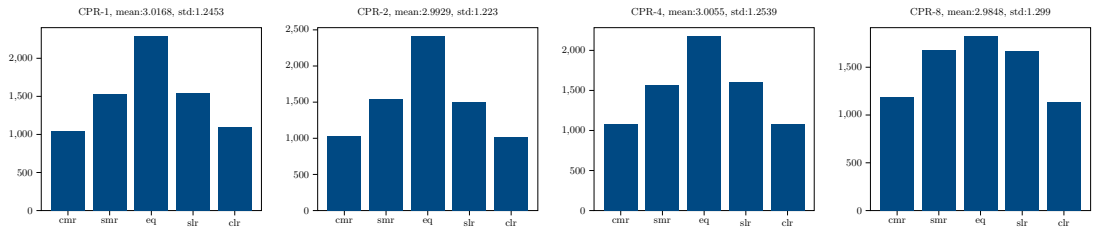


Fig. 15: The distribution of each stacked bar from Figure 7.

C Additional Material from Experiment 2

Figures 16 (CPR 4), 17 (CPR 8), and 18 (CPR 32) complement the previous confusion matrices presented in section 4.3. Darker values indicate lower numbers,

lighter values indicate higher numbers. The diagonals display correct classifications, while the right-most column shows the number of 'I don't know / None of the above'.

Together with CPR 8, CPR 4 has the highest error-rate (5.36%). The highest indecisiveness and error-rate is given for class 'chain saw' across all CPR. CPR 8 demonstrated the lowest accuracy in experiment 2 (81.2%). CPR 32 achieved the highest indecisiveness (14.2%) and second lowest accuracy in experiment 2 (81.32%). To summarize, table 9 provides an overview of indecisiveness per class and CPR.

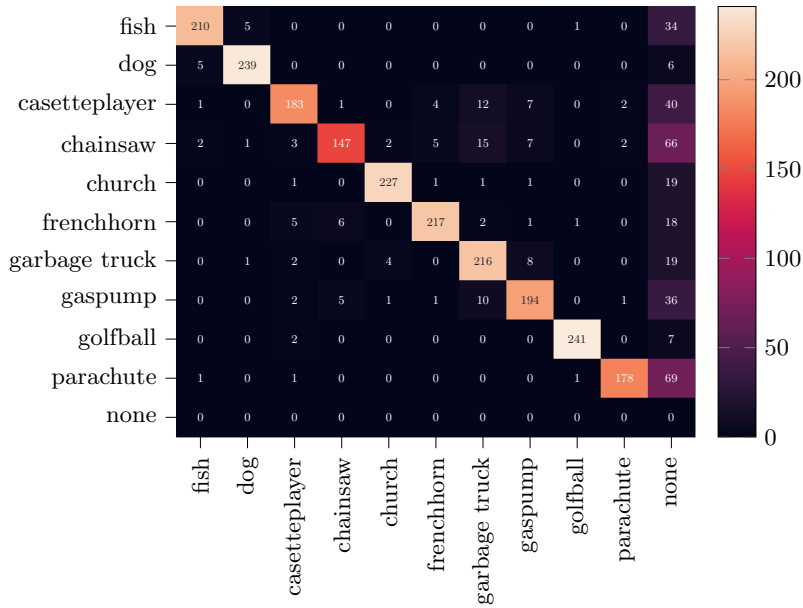


Fig. 16: Confusion Matrix CPR 4.

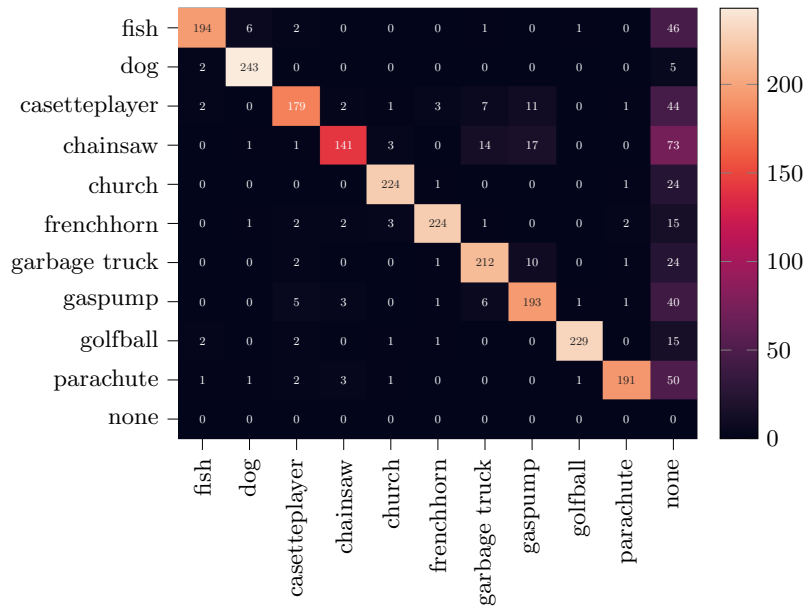


Fig. 17: Confusion Matrix CPR 8.

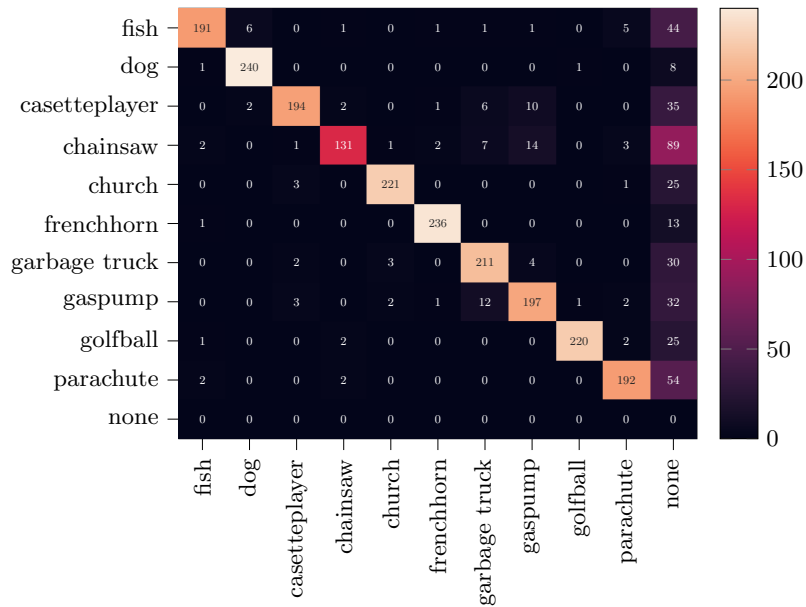


Fig. 18: Confusion Matrix CPR 32.

	CPR 1	CPR 2	CPR 4	CPR 8	CPR 32
fish	6.8%	7.2%	13.6%	18.4%	17.6%
dog	8.8%	4.0%	2.4%	2.0%	3.2%
cassetteplayer	13.2%	12.0%	16.0%	17.6%	14.0%
chainsaw	22.4%	22.0%	26.4%	29.2%	35.6%
church	12.8%	3.6%	7.6%	9.6%	10.0%
frenchhorn	4.0%	3.2%	7.2%	6.0%	5.2%
garbagetruck	7.2%	5.2%	7.6%	9.6%	12.0%
gaspump	11.6%	14.8%	14.4%	16.0%	12.8%
golfball	2.4%	1.6%	2.8%	6.0%	10.0%
parachute	8.8%	16.0%	27.6%	20.0%	21.6%
total	9.80%	8.96%	12.56%	13.44%	14.20%

Table 9: Indecisiveness of the respondents per class for all CPRs.